Supplementary data

Abnormal brown adipose tissue mitochondrial structure and function in IL10 deficiency

José C. de-Lima-Júnior[1,2], Gabriela F. Souza[1,2], Alexandre Moura-Assis[1,2], Rodrigo S. Gaspar[2,3], Joana M. Gaspar[1,2], Andréa L. Rocha[4], Danilo L. Ferrucci[5,6], Tanes I. Lima[2,4], Sheila C. Victório[1,2], Ivan L. P. Bonfante[7], Claudia R. Cavaglieri[7], José C. Pareja[8], Sérgio Q. Brunetto[9], Celso D. Ramos[2,10], Bruno Geloneze[2,8], Marcelo A. Mori[4], Leonardo R. Silveira[2,4], Gesmar R. S. Segundo[11], Eduardo R. Ropelle[2,3], Lício A. Velloso[1,2]*

Materials and methods

PET/CT image analyse in mice

Images were acquired and processed using ALBIRA, a small animal PET⁄SPECT⁄CT in vivo imaging system (Bruker® Corporation, Massachussetts, USA) and analyzed using a PMOD workstation, also from Bruker®. (18F)-FDG was obtained from the Nuclear and Energy Research Institute (IPEN, Sao Paulo, Brazil). Mice were anesthetized with 2% isoflurane and injected in the venous sinus with 5 MBq of 2-deoxy-2-[18F]fluoro-d-glucose ([18F]FDG). Mice were keep awake and exposed at 4 ˚C during uptake period of 60 minutes. The computed tomography was performed as a low-dose acquisition with 80 kVp, 160 µA, and 1024 projections, during 0.8s per CT rotation, pitch 4.0 – 5.0 mm, field of view of 71.3mm and a scan speed of 24.6 mm/s. The PET scan was performed immediately after the CT scan without changing the position of the mice, always in the craniocaudal direction from head to proximal thighs. After 60 minutes of [18F]FDG uptake, PET scans were started for a total duration of 40 min. PET scans were reconstructed using the PMOD in LabPET software and images were calibrated in Bq per mL by scanning a phantom cylinder. Regions of interest (ROI) were drawn on surrounding slices on CT scans and reconstructed as three-dimensional volumes to measure densities and uptake of each desired tissue. Then, PET images were processed and converted

into standardized uptake values (SUVs) adjusted by body weight of each animal and superimposed on the CT anatomical image to measure [18F]FDG uptake in the indicated tissue.

***In vivo* Multiphoton Redox and Fluorescence Lifetime Imaging (FLIM)**

Before imaging, the mice were anesthetized with an intraperitoneal injection of a mixture of ketamine (200mg / kg), xylazine (5mg / kg) and diazepam, and the interscapular BAT was dissected rapidly and then minced into very small fragments in a chambered coverglass for acquiring images. The multiphoton images were obtained with the Zeiss LSM780-NLO com Becker&Hickl Photon Counting at the University of Campinas. The source was a titanium sapphire laser. A FLIM image z-stack was collected from the same tissue volume at 890-nm excitation. Single photon counting was accomplished at a rate of 5 x 10^4 photons per second. We used SPCImage software (Becker and Hickl) to evaluate the fluorescence lifetime decay curves. The redox ratio was calculated dividing FAD fluorescence intensity by NADH fluorescence intensity, pixel by pixel, using ImageJ.

Quantitative RT-PCR

Total RNA was extracted from mouse BAT by using TRIzol reagent (Invitrogen) according to the manufacturer's recommendations. The cDNA synthesis was performed using 2.0 µg of total RNA according the manufacturer's instructions (High Capacity cDNA Reverse Transcription Kit, Life Technologies). Each PCR contained 25–40 ng of reverse-transcribed RNA, 0.25 µl of each specific primer, Taqman Universal master mix (Life Technologies), and RNAse-free water to a 10 µl final volume. Real time PCR analysis of gene expression was carried out in an ABI Prism 7500 sequence detection system (Applied Biosystems). Primers were purchased from Applied Biosystems or Integrated DNA Technologies. Relative gene expression was normalized to that of GAPDH in all samples according to the ΔΔCt method. Real-time data were analyzed using the Sequence Detector System 1.7 (Applied Biosystems). The nucleotide sequences of the primers are: Pgc-1α - Forward primer (5'-3') – AGCCGTGACCACTGACAACGAG and Reverse

primer (5'-3') – GCTGCATGGTTCTGAGTGCTAAG; Ucp1 - Forward primer (5'-3') GGCCTCTACGACTCAGTCCA and Reverse primer (5'-3') – TAAGCCGGCTGAGATCTTGT.

Rectal temperature and interscapular brown adipose tissue thermal release

To evaluate core temperature we performed the measurements using a digital thermometer (BAT-7001H, Clifton, NJ, USA) in combination with a copper-constantan thermocouple rectal probe (RET-3) obtained from Physitemp Instruments (Clifton, NJ, USA). The probe was petroleum jelly-lubricated before being positioned in the rectum at 2-2.5 cm for 1 second. Measurements were taken every hour after exposure to cold. For the detection of interscapular brown adipose tissue thermal release, an infrared (IR) camera (FLIR T450sc, FLIR Systems, Inc. Wilsonville, USA) was employed to obtain surface images of each mouse with an IR resolution of 320 × 240 pixels and a Thermal sensitivity / NETD of <40 mK @ +30 ° C (+ 86 ° F). Images were presented in rainbow high contrast form available in the color palette of the free software FLIR Tools IR.

Metabolic phenotyping and locomotor activity.

The physiological markers of energy expenditure (O_2 consumption, CO_2 production, RER, heat rate, and ambulatory activity) were measured using an open circuit calorimeter system, the LE405 Gas Analyzer (Panlab – Harvard Apparatus, Holliston, MA, USA), which was calibrated as recommended by the manufacturer. Mice were acclimated for 24 h in the apparatus, and thereafter, data were recorded for 24 h (light and dark periods).

Supplementary Figures

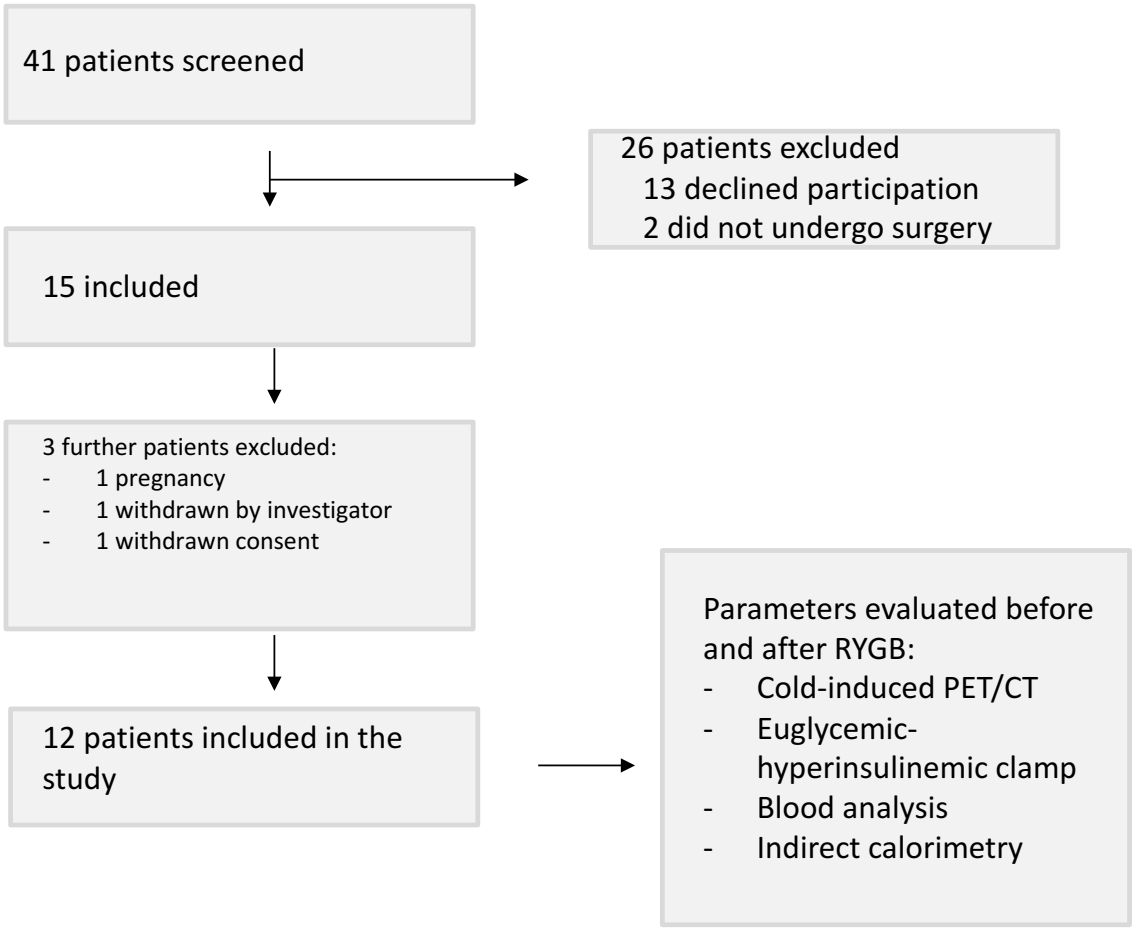

Supplementary Figure 1. Flow diagram of obese volunteers submitted to Roux-in-Y gastric bypass (RYGB).

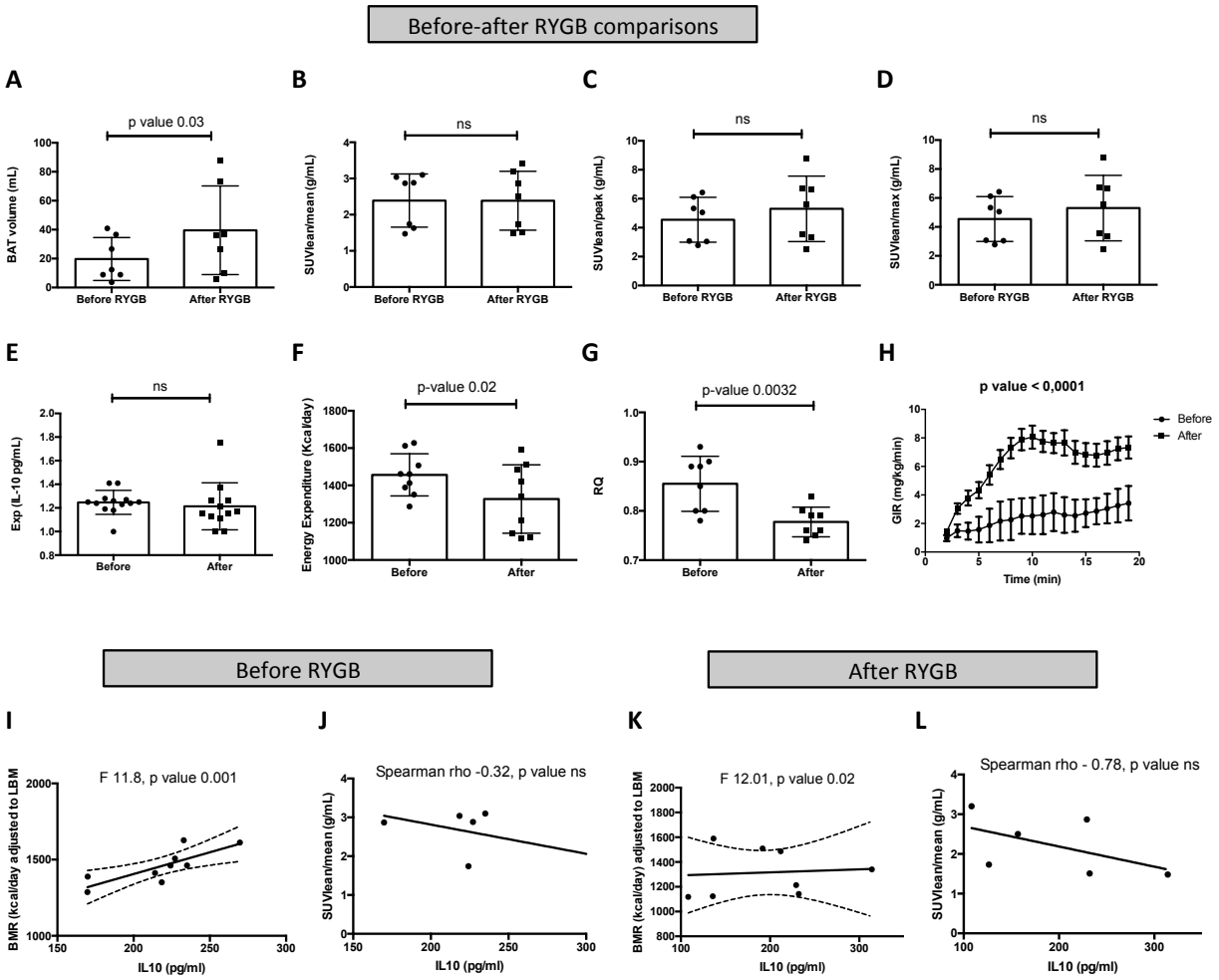

Supplementary Figure 2. IL10 is associated with energy expenditure, but not with BAT metabolic activity in obese individuals underwent bariatric surgery (RYGB). A-**D**, Comparison of BAT metabolic activity before and after RYGB (n=7). **A**, BAT volume; **B**, $SUV_{lean/mean}$; **C**, $SUV_{lean/peak}$; **D**, $SUV_{lean/max}$. **E**-**H**, Comparison of inflammatory/metabolic parameters before and after RYGB (n=8-12). **E**, Serum IL10 levels; **F**, energy expenditure; **G**, respiratory quotient; **H**, glucose infusion rate during euglycemic hyperinsulinemic clamp. **I**-**L**, Correlation of serum levels of IL10 and BAT metabolic activity or energy expenditure in obese individuals before RYGB (n=7-8). **I**, Serum IL10 levels versus energy expenditure using generalized linear models with estimated lean body mass; **J**, serum IL10 levels versus $SUV_{lean/mean}$ (2 data points are outside of the axis limits). **K**-**L**, Correlation of serum IL10 and BAT metabolic activity or energy expenditure in obese subjects after RYGB (n=7-8). **K**, Serum IL10 levels versus energy expenditure using generalized linear models with estimated LBM; **L**, Serum IL10 levels versus $SUV_{lean/mean}$ (2 data points are outside of the axis limits).

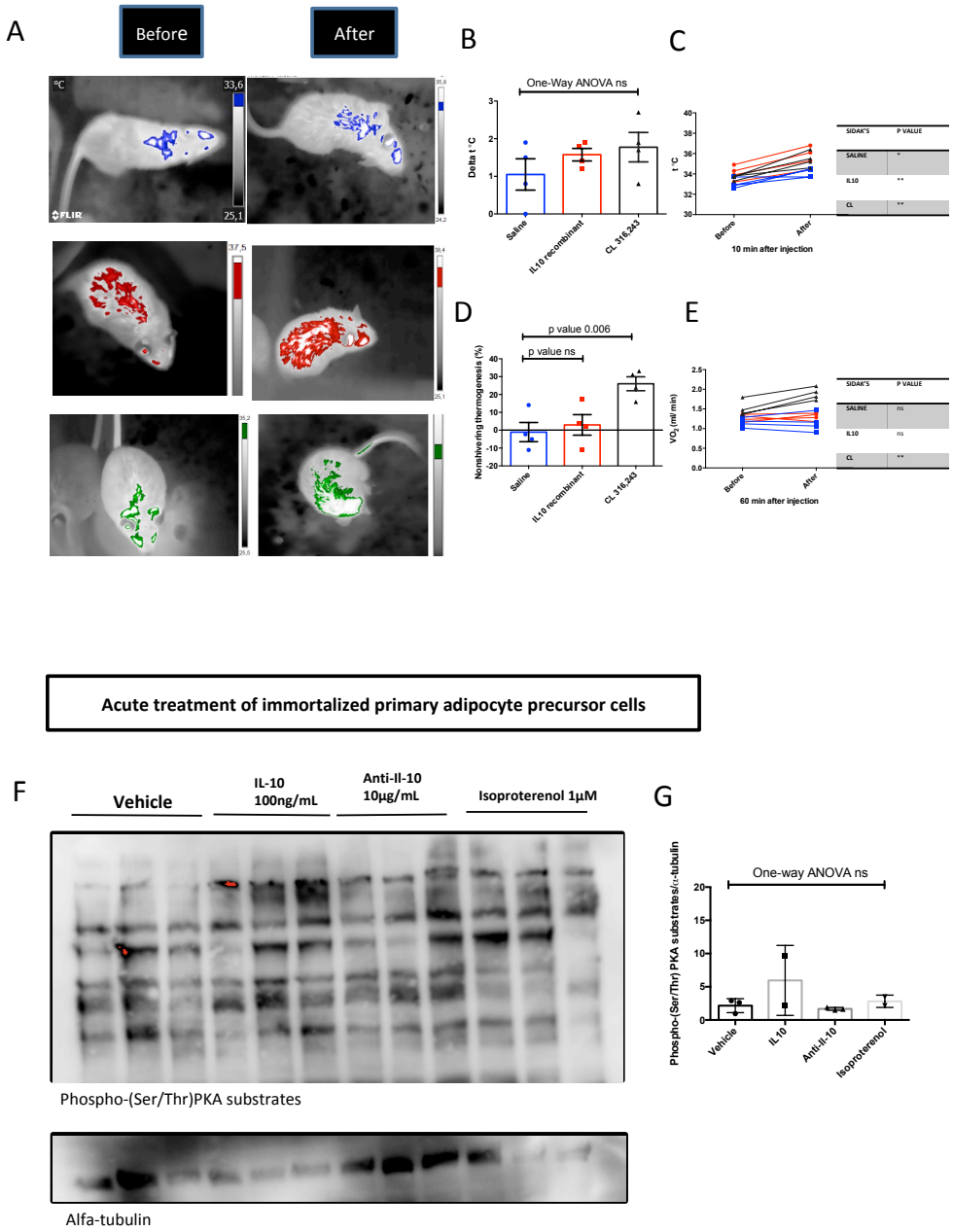

Supplementary Figure 3. No acute thermogenic response to IL10 treatment. Male WT mice were treated with saline, recombinant IL10 (10 µg/kg/dose) or the β_3-agonist CL316,243 (1mg/kg/day) to evaluate acute thermogenic response after IL10. **A**, Representative surface infrared iBAT temperature image before and after indicated treatment. **B**, Surface infrared iBAT temperature before and after indicated treatment. **C**, Surface infrared iBATdelta temperature before and after indicated treatment. **D**, Whole body O_2 consumption before and after indicated treatment. **E**, Nonshivering thermogenesis calculated from (**D**) data. **F**, Acute treatment of immortalized primary brown adipocyte precursor cells. Western blot representative image measuring Phospho-(Ser/Thr) PKA Substrates after indicated treatments. **G**, Densitometry quantification of Phospho-(Ser/Thr) PKA Substrates normalized by alfa tubulin. N = 3 per condition. Ordinary one-way ANOVA was performed.

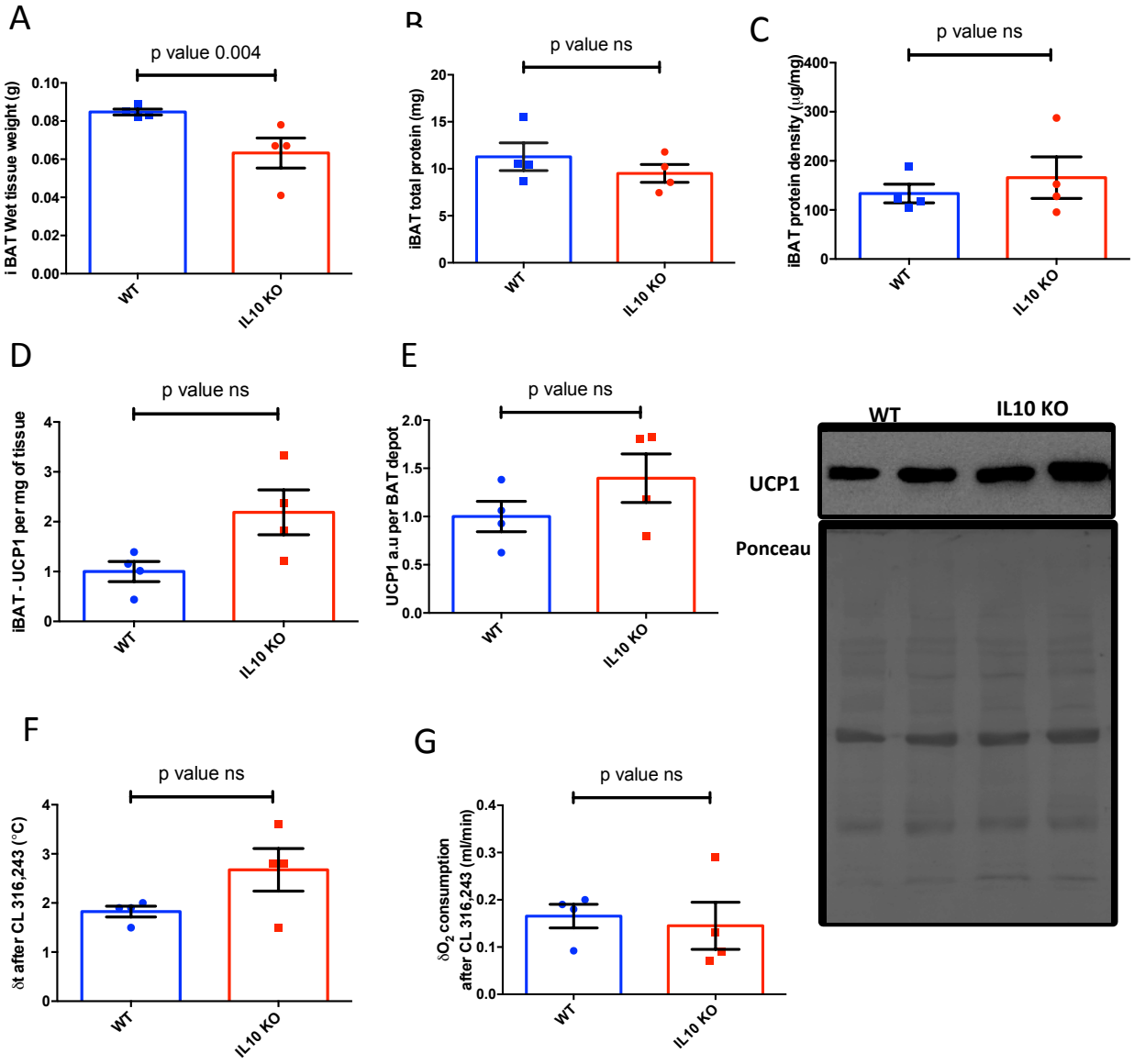

Supplementary Figure 4. IL10 KO mice have preserved thermogenic capacity. **A**, Wet tissue weight of BAT. **B**, iBAT total protein content. **C**, iBAT protein density. **D**, UCP1 per mg of tissue. **E**, UCP1 total content per depot calculated as **B** multiplied by **C**. WT was normalized to 1. The Representative western blot image measuring UCP1 is depicted in the right-hand bottom corner of the figure. N = 4 per condition. *After stripping, this membrane was the same used to blot anti-OPA1 and Mfn 2 (Fig. 4H), TFAM and OXPHOS (Supp. Fig. 6 A). The loading control used is the same, as indicated in supplementary material with details about cut blots.* **F**, Change in iBAT temperature during a BAT thermogenic capacity analysis using CL-induced thermogenesis test in awake mice. G, Change in O2 consumption during a BAT thermogenic capacity analysis using CL-induced thermogenesis test in awake mice. Data indicate means ± SEM. N = 4 mice per condition. Student's unpaired t-test was performed. * p< 0.05

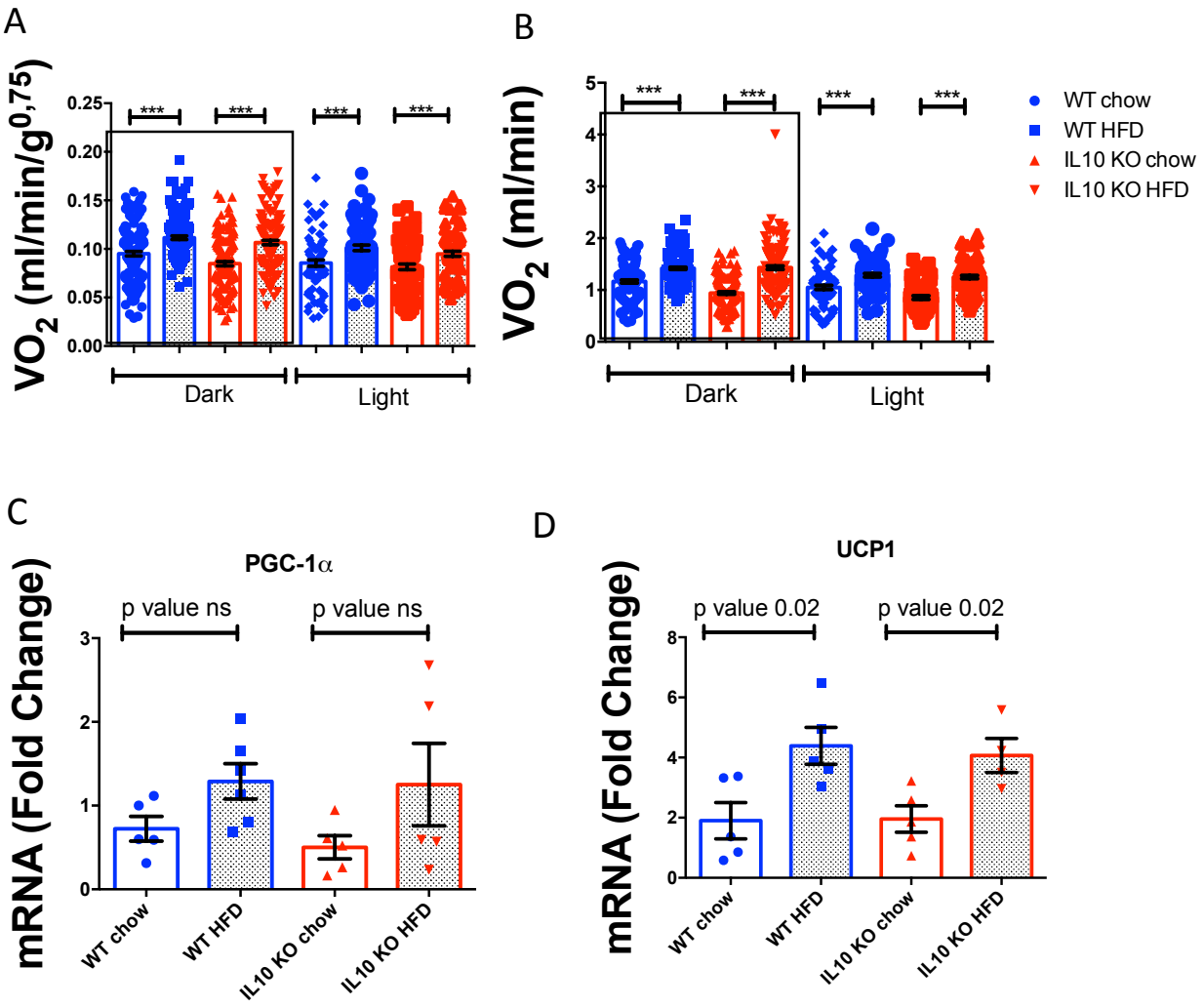

Supplementary Figure 5. IL10 KO mice have preserved diet-induced thermogenesis. **A-B**, Effect of high-fat diet on oxygen consumption (VO_2) in awake male WT mice. N = 4. **C**, Effect of high-fat diet on PGC-1α mRNA levels in awake male WT mice and IL10KO mice. N = 5 per condition. **D**, Effect of high-fat diet on Ucp1 mRNA levels in awake male WT mice and IL10KO mice. N = 5 per condition. Data indicate means ± SEM. $^{*}p \leqslant 0.05$; $^{**}p \leqslant 0.01$; $^{***}p \leqslant 0.001$, Statistical analysis was performed using Student's unpaired t test.

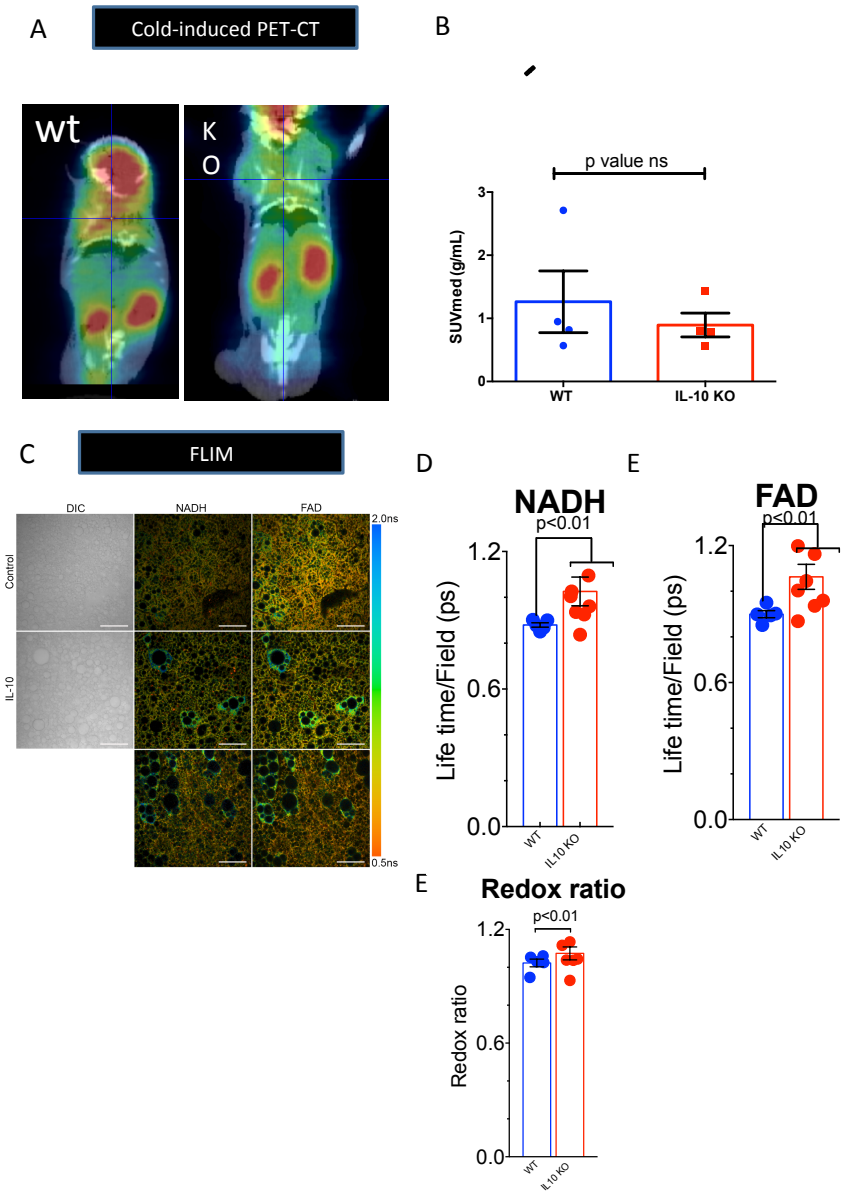

Supplementary Figure 6. Assessment of iBAT glycolysis using ^{18}F-FDG PET/CT and analysis of metabolic status using FLIM. A, Representative image and quantification of 2h cold-stimulated iBAT ^{18}F-FDG uptake (SUVmax) in WT and IL10 KO mice. **B**, Representative fluorescence lifetime imaging obtained using ex vivo iBAT from WT and IL10 KO mice. **C**, FLIM of autofluorescent NADH. **D**, FLIM of autofluorescent FAD. **E**, Reduction-oxidation pair NADH:NAD+ (redox ratio) between WT and IL10 KO mice. In **A**, n = 4. In **B-E**, n = 5. Data indicate means ± SEM. **p ⩽ 0.01. Statistical analysis performed using Student's unpaired t test.

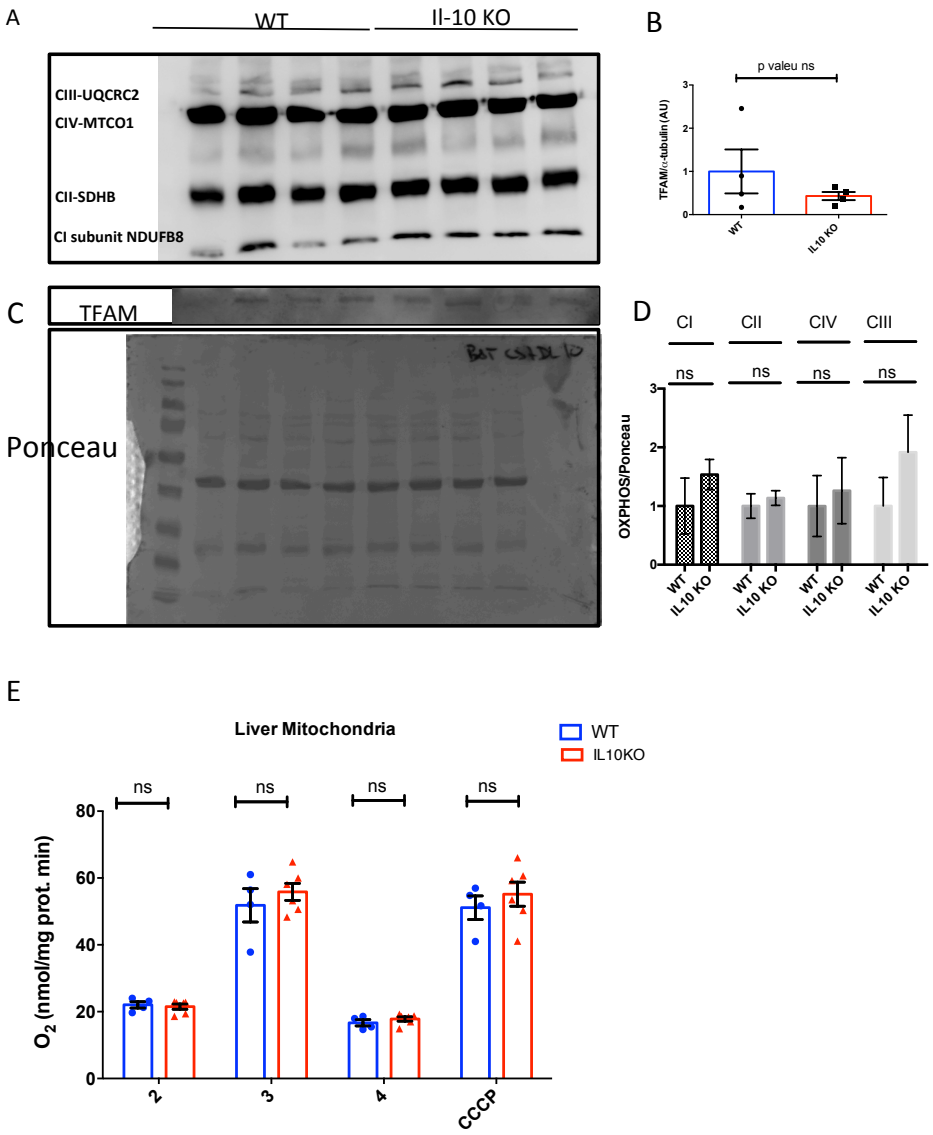

Supplementary Figure 7. Analysis of OXPHOS complex proteins and liver mitochondria respiration. A-D, Representative Western blot image of OXPHOS complex proteins and TFAM in iBAT from WT and IL10 KO mice. N = 4 per condition. *After stripping, this membrane was the same used to blot anti-OPA1 and Mfn 2 (Fig. 4H), and anti-UCP1 (Supp. Fig. 4E). The loading control used is the same, as indicated in supplementary material with details about cut blots.* N = 4 per condition. **E**, Quantification of complex I-driven (pyruvate-malate) oxygen consumption rates (OCR) in liver isolated mitochondria from wild type (WT) and IL10 KO mice. State 2 quantifies no-ATP synthesis-related respiration (proton leak). State 3 quantifies OCR coupled to maximal ATP synthesis. State 4oligo quantifies rate of basal non-phosphorylating oxygen consumption after oligomycin and state 3u quantifies maximal respiration induced by FCCP. Bar graphs show average ± SEM per experiment (n= 3 - pool of 3 mice per group). Statistical analysis was performed using Student's t-test, unpaired; two-way ANOVA was performed using Sidak's test, $p< 0.05$.

Supplementary Tables

Supplementary Table 1. Clinical trials on going targeting brown adipose tissue

Study title	Identifier	Intervention
Longitudinal Follow-up of Brown Adipose Tissue Function and Structure	NCT01985503	Observational
The Effects of Capsinoids on Brown Adipose Tissue Activation in Obesity	NCT03110809	Capsinoid vs placebo
Study of the Effect of Vagus Nerve Stimulation on Human Brown Adipose Tissue Activity	NCT01491282	Enabling and disabling vagal nervous system
STAGES Trial: Study of Adiposity, Growth and Endocrine Stages	NCT01460784	Observational
Dopaminergic Effects on Brown Adipose Tissue	NCT02428933	Bromocriptine
CB1 Receptors in Human Brown Adipose Tissue	NCT02941172	Observational
Brown Adipose Tissue and Body Mass Index	NCT02173834	Observational
Detection of Brown Adipose Tissue by Magnetic Resonance Imaging (BAT_PET/MRI)	NCT02237872	Observational
Secretin Activates Human Brown Adipose Tissue.	NCT03290846	Secretin
Effects of b3-Adrenergic Receptor Agonists on Brown Adipose Tissue	NCT01783470	Mirabegron
The Detection and Factors of Brown Adipose Tissue in Different Locations of Adults	NCT01387451	Observational
Hyperpolarized Xenon-129 Magnetic Resonance Imaging and Spectroscopy of Brown Fat: Healthy Adult Volunteer Pilot Study	NCT02220426	Observational
Mirabegron and Brown Adipose Tissue	NCT03012113	Mirabegron
The Incidence and Factors of Brown Adipose Tissue in Chinese	NCT01381042	Observational
The Incidence,Factors,and Importance of Brown Adipose Tissue in Chinese Adults	NCT01387438	Observational
Exenatide and Brown Adipose Tissue (exe01)	NCT03002675	Exenatide
Adenosine and A2A Receptors in Human Brown Adipose Tissue	NCT03327168	Adenosina
The Role of Brown Adipose Tissue in Triglyceride Clearance in People	NCT02786251	Observational
Activation of Cervical and Upper Thoracic Brown Adipose Tissue in Humans Via Beta-adrenergic	NCT01015794	Ephedrine Hydrochloride

Stimulation		
Brown Adipose Tissue Activity and Age	NCT02130154	Observational
Influence of Liraglutide, a GLP-1 Receptor Agonist, on Brown Adipose Tissue (BAT) Activity in Humans	NCT02718950	Liraglutide
Brown Fat Activity and Bariatric Surgery	NCT03168009	Bariatric surgery
Brown Adipose Tissue Activity in Pre- and Postmenopausal Women	NCT02927392	Leuprolide acetate
The Effect of Brown Adipose Tissue Activation on Insulin Sensitivity in Humans	NCT01791114	Observational
GLP-1 Agonism Stimulates Browning of Subcutaneous White Adipose Tissue in ObesityMen	NCT02170324	Exenatide
Effects of Sleep Restriction on BAT Activation in Humans	NCT02770118	Sleep deprivation
Calorie Restriction Retards the Aging Process	NCT01508091	Calorie restriction
Monounsaturated Fatty Acids and Brown/Beige Adipose Tissue in Humans	NCT03024359	Extra virgin olive oil
Brown Adipose Tissue Activity and Thyroid Hormone	NCT02499471	Levothyroxine therapy
Enhancement of Brown Adipose Tissue Function Via Chronic Pharmacological Treatment	NCT02236962	Placebo, Ephedrine and pioglitazone
Activating Brown Adipose Tissue Through Exercise	NCT02365129	Exercise training
A Role for Brown Adipose Tissue in Postprandial Thermogenesis?	NCT01974778	Meal
Studying the Effect of Capsinoids on Brown FatUsing Infrared Thermal Imaging.	NCT01961674	Capsinoid/placebo and rice
BRown Fat Activity Measurement With Infrared imaginG tHermography andThermogenesis - the BRIGHT Study	NCT02790255	Observational
Chronic Intermittent Cold Exposure on Weight Loss	NCT01312090	Whole-body cryotherapy
Efficacy of Pharmacological Stimulation of BAT and WAT in Lean and Obese Young Adults	NCT02354807	Mirabegron
Effects of Hyperthyroidism on Amount and Activity of Brown Adipose Tissue	NCT02133040	Observational
Collection of Human Tissue Samples From the Neck Region for Characterization of Its Molecular and Biochemical Signatures	NCT02274805	Observational
Effects of Estrogen Deficiency on Energy Expenditure	NCT01846728	Estrogen supression
Leipzig Adipose Tissue Childhood Cohort	NCT02208141	Observational
Human Brown Adipose Tissue and Mitochondrial Respiration	NCT03111719	Observational
Cold Stress Stimulate the Browing of Subcutaneous White Adipose in Healthy Adults	NCT02159144	Cold stress

Brown Fat Activation Study	NCT02919176	Mirabegron and pioglitazone
Nicotinamide Riboside and Metabolic Health	NCT02835664	Nicotinamide Riboside (Niagen)
Sildenafil Activates Browning of White Adiposeand Improves Insulin Sensitivity	NCT02524184	Sildenafil
Energy Expenditure Responses to Different Temperatures	NCT01568671	Different temperatures
Cold Induced Activation of Brown Adipose Tissue in Humans	NCT03096535	Cold stress
Correlation of Irisin and Adipokine Levels With Body Mass Index and Risk Factors for Metabolic Syndrome in Hispanic Children	NCT02320110	Observational
Physiological Responses and Adaptation of Brown Adipose Tissue to Chronic Treatment With Beta 3-Adrenergic Receptor Agonists	NCT03049462	Mirabegron
A Cold Physical Treatment to Manage Insulin Resistance	NCT02852759	Selective Cold treatment and Electroacupuncture

Supplementary Table 2. Baseline data for clinical variables of middle-aged diabetic subjects

Variable	Baseline
Number of subjects	16
Age, yr	52 (7,75)
Female sex, %	100
Diabetes, %	100
Weight, kg - Mean (95% CI)	83,8 (10,53)
BMI, kg/m^2	29,3 (4,76)
Glucose, mg/dL - Mean (95% CI)	137 (49)
Insulin, mUI/mL - Mean (95% CI)	9,8 (7,63)
HbA1C, %	6,95 (1,75)
HOMA2-IR	1,33 (1,13)
BAT volume, mL - Mean (95% CI)	6,2(14,21)
$SUV_{lean/mean}$, g/mL	2,18 (0,49)
$SUV_{lean/max}$, g/mL	3,46 (2,24)
$SUV_{lean/peak}$, g/mL	2,86 (1,96)
LDL cholesterol, mg/dL -Mean (95% CI)	121 (52,75)
HDL cholesterol, mg/dL - Mean (95% CI)	37,5 (13,25)
Triglycerides, mg/dL - Mean (95% CI)	121,5 (91,75)
Total cholesterol, mg/dL - Mean (95% CI)	199 (59,75)

To convert glucose to millimoles per liter, multiplies by 0.01129. Lean body mass was obtained using pletismography for correction of SUV in PET imaging. To convert cholesterol to millimoles per liter, multiplies by 0.02586. To convert triglycerides to millimoles per liter, multiplies by 0.01129. CI, confidence interval; SUV, standardized uptake value; LDL, low-density lipoprotein; HDL, high-density lipoprotein.

Supplementary Table 3. Unadjusted baseline and 1-year follow-up for clinical variables

Variable	Before surgery	After surgery
Age, yr	36.2 (32.7 – 39.8)	37.5 (34.0 – 41.1)
Female sex, %	100	100
Weight, kg Mean (95% CI)	108.41 (100.66 – 116.16)	80.48*** (76.85 – 84.11)
Change from baseline, % Mean (95% CI)		-25.90 (-30.54 - -21.26)
Glucose, mg/dL Mean (95% CI)	91.56 (82.78 – 100.34)	77.72*** (71.27 – 84.19)
Insulin, mUI/mL Mean (95% CI)	17.21 (11.05 – 23.39)	4.69** (2.88 – 6.51)
M-value 120-180 Mean (95% CI)	2.95 (2.30 – 3.60)	7.13** (5.30 – 8.98)
SUV, g/mL Mean (95% CI)	2.88 (-0.60 – 7.33)	4.65 (0.68 – 8.64)
LDL cholesterol, mg/dL Mean (95% CI)	107 (85.80 – 128.20)	75.73* (54.88 – 96.59)
HDL cholesterol, mg/dL Mean (95% CI)	45 (40.11 – 49.90)	51.73 (40.59 – 62.88)
Triglycerides, mg/dL Mean (95% CI)	83.11 (53.69 – 112.54)	66 (47.57 – 84.43)
Total cholesterol, mg/dL Mean (95% CI)	169.78 (149.85 – 189.70)	139.55* (117.88 – 157.22)
CRP, mg/dL Mean (95% CI)	18.33 (-14.63 – 51.28)	4.09** (-2.14 – 10.30)

All patients were submitted to RYGB. The sample size does not include data from patients who lost follow-up. We performed Wilcoxon matched-pairs signed rank test. No adjustments were performed for multiple comparisons. To convert glucose to millimoles per liter, multiplies by 0.01129. To convert cholesterol to millimoles per liter, multiplies by 0.02586. To convert triglycerides to millimoles per liter, multiplies by 0.01129. CI, confidence interval; SUV, standardized uptake value; LDL, low-density lipoprotein; HDL, high-density lipoprotein. *p<0,05, **p<0,01, ***p<0,001

Unspliced immunoblot images used in this study and raw data analysis

Figure 4G – Opa1

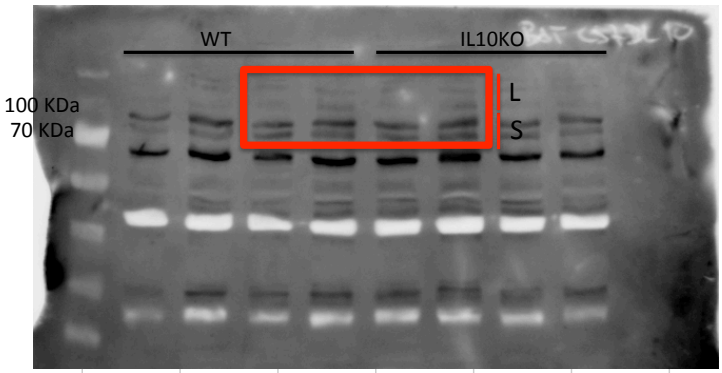

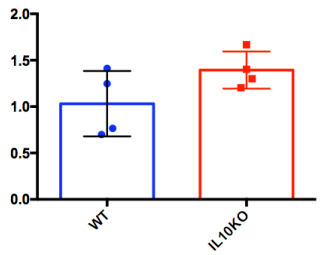

OPA1 ratio to longer form

wt - long	wt short	
23962	18351	0,76583758
30650	21412	0,69859706
20414	28819	1,41172725
28646	35749	1,24795783

KO - long	ko short	
19718	32877	1,66735977
30101	39168	1,30121923
14690	20607	1,40279101
19057	22940	1,20375715

Unpaired t test with equal SD

		A
		Data Set-A
		Y
1	Table Analyzed	Opa1-S/L
2		
3	Column B	IL10KO
4	vs.	vs.
5	Column A	WT
6		
7	Unpaired t test	
8	P value	0.1235
9	P value summary	ns
10	Significantly different? (P < 0.05)	No
11	One- or two-tailed P value?	Two-tailed
12	t, df	t=1.791 df=6
13		

FIGURE 4 G – Mfn2

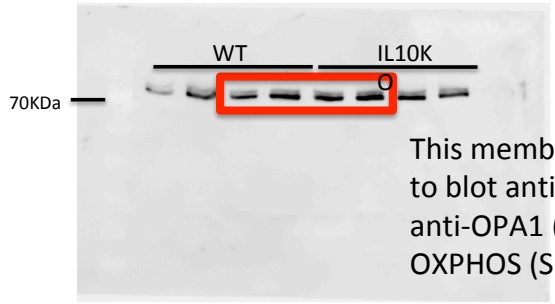

This membrane was stripped to blot anti-UCP1 (Supp. Fig. 3E), anti-OPA1 (Fig. 4H), TFAM and OXPHOS (Supp. Fig. 6 A).

Ponceau

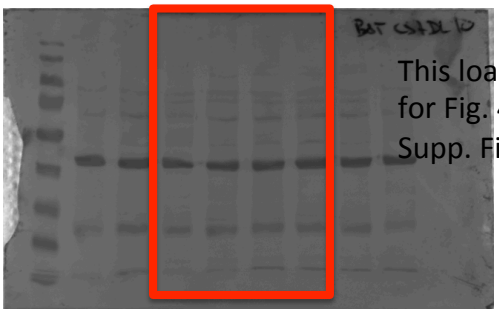

This load control was used for Fig. 4H, Supp. Fig. 3E and Supp. Fig. 6 A.

Unpaired t test with equal SD		A
		Data Set-A
		Y
1	Table Analyzed	Mfn2
2		
3	Column B	IL10KO
4	vs.	vs.
5	Column A	WT
6		
7	Unpaired t test	
8	P value	0.4181
9	P value summary	ns
10	Significantly different? (P < 0.05)	No
11	One- or two-tailed P value?	Two-tailed
12	t, df	t=0.8693 df=6
13		
14	How big is the difference?	
15	Mean ± SEM of column A	0.7318 ± 0.1633 N=4
16	Mean ± SEM of column B	0.4950 ± 0.2179 N=4
17	Difference between means	-0.2367 ± 0.2723
18	95% confidence interval	-0.9031 to 0.4296
19	R squared	0.1119
20		
21	F test to compare variances	
22	F,DFn, Dfd	1.782, 3, 3
23	P value	0.6470
24	P value summary	ns
25	Significantly different? (P < 0.05)	No

H18

	A	B	C	D	E	F	G
1	Mfn2						
2							
3							
4	Segment	Area		Ponceau	Area_all peak:	Mfn_Ponceau	
5	1	2.037.548	wt	wt	5.834.644	0,34921548	
6	2	4.650.711	wt	wt	7.114.905	0,6536575	
7	3	3.839.468	wt	wt	4.879.451	0,78686475	
8	4	5.583.317	wt	wt	4.909.358	1,13728048	
9	5	881.284	ko	ko	5.369.188	0,1641373	
10	6	1.702.719	ko	ko	5.894.673	0,28885724	
11	7	2.045.355	ko	ko	5.197.480	0,39352821	
12	8	6.021.447	ko	ko	5.312.066	1,13354145	
13							
14							
15							
16							

FIGURE 4J

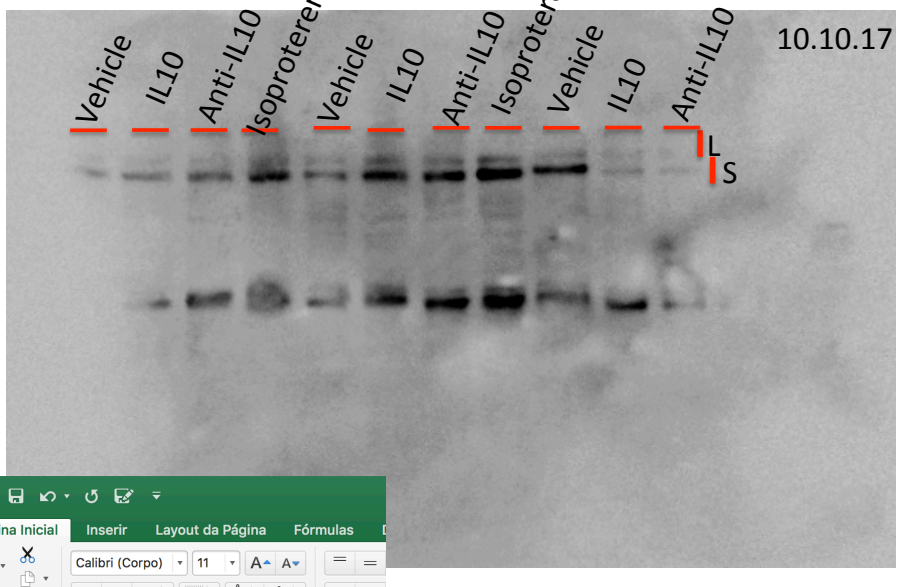

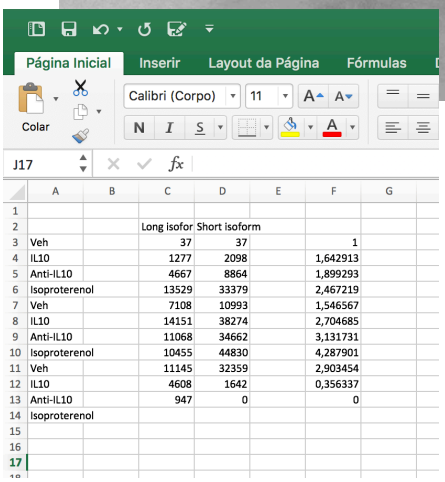

	A	B	C	D	E	F	G
1							
2			Long isofor	Short isoform			
3	Veh		37	37		1	
4	IL10		1277	2098		1,642913	
5	Anti-IL10		4667	8864		1,899293	
6	Isoproterenol		13529	33379		2,467219	
7	Veh		7108	10993		1,546567	
8	IL10		14151	38274		2,704685	
9	Anti-IL10		11068	34662		3,131731	
10	Isoproterenol		10455	44830		4,287901	
11	Veh		11145	32359		2,903454	
12	IL10		4608	1642		0,356337	
13	Anti-IL10		947	0		0	
14	Isoproterenol						
15							
16							
17							

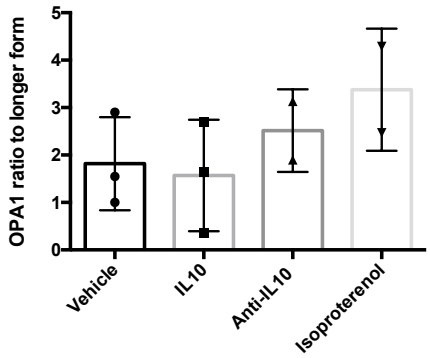

Ordinary one-way ANOVA		A	B
		Data Set-A	Data Set-B
		Y	Y
1	Table Analyzed	Data 1	
2			
3	ANOVA summary		
4	F	1.298	
5	P value	0.3582	
6	P value summary	ns	
7	Are differences among means statistically significant? (P < 0.05)	No	
8	R square	0.3936	
9			

SUPP. FIG. 3F

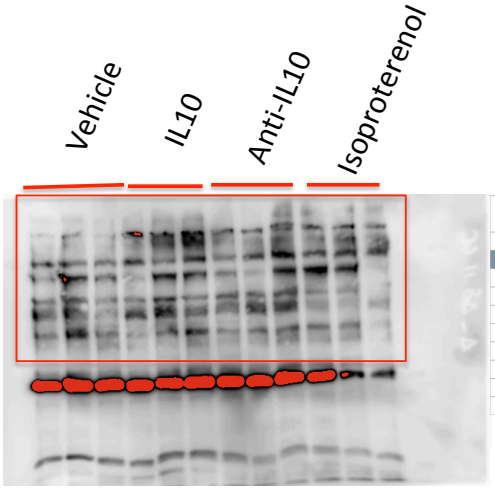

Ordinary one-way ANOVA	A
	Data Set-A
	Y
1 Table Analyzed	Data 1
2	
3 ANOVA summary	
4 F	1.607
5 P value	0.2839
6 P value summary	ns
7 Are differences among means statistically significant? (P < 0.05)	No
8 R square	0.4455
9	

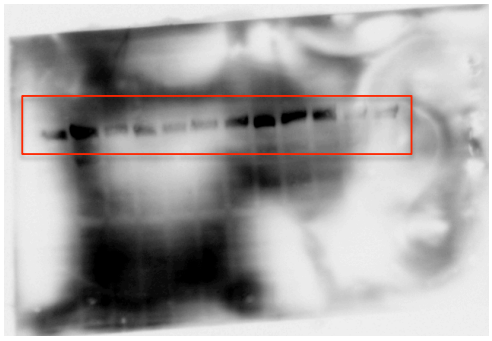

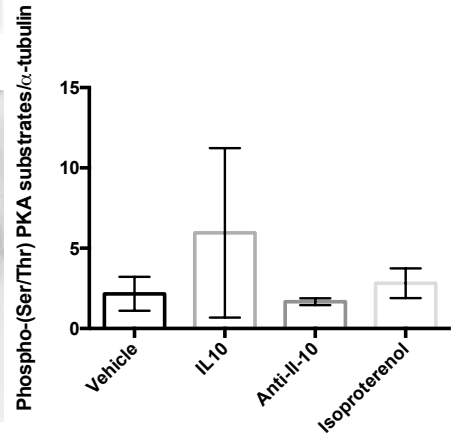

K	L	M	N	O	P	Q	R	S	T	U	V	W
lane 1	2	3	4	5	6	7	8	9	10	11	12	
134.971	337.406	173.263	1.965.355		273.506	540.406	606.577		744.577	598.627	447.042	
1.605.962	1.527.083	1.133.648	1.848.012	395.991	1.587.861	856.355	1.417.841	504.627	207.920	359.335	1.450.154	
1.005.598	3.834.740	1.518.719	615.284	684.598	2.350.134	992.305	299.092	1.962.012	1.198.527	1.080.184	674.991	
590.770	1.065.255	518.062	725.012	3.324.326	800.770	634.891	359.163	2.065.891	3.983.326	2.429.790	269.021	
1.736.719	1.171.234	279.435	2.013.912	698.577	1.288.234	979.891	2.152.497	375.627	232.092	366.506		
1.096.012	2.780.690	599.456	259.971	1.895.719	1.632.598	480.820	643.941	1.986.861	836.820	445.163		
				1.204.376				238.971				
6.170.032	10.716.408	4.222.583	7.427.546	8.203.587	7.933.103	4.484.668	5.479.111	7.133.989	7.203.262	5.279.605	2.841.208	PKA
2.354.083	3.685.861	4.411.317	3.333.276	220.092	819.355	2.354.083	3.685.861	4.411.317	3.333.276	220.092	819.062	alfa-tubulina
2,6209917	2,90743682	0,95721595	2,22830213	37,2734447	9,68213168	1,90505942	1,48652133	1,61720162	2,16101577	23,9881731	3,46885584	

SUPP. FIG. 4D-4E

UCP1

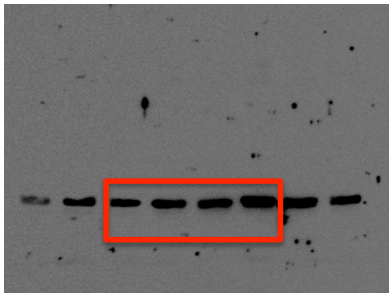

Ponceau

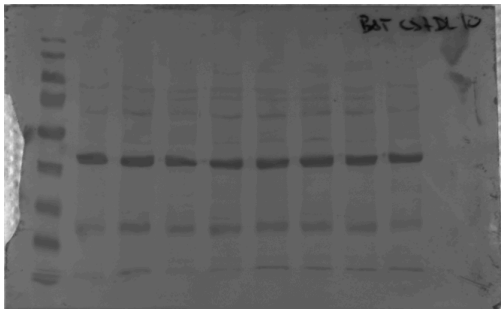

I20

	A	B	C	D	E	F	G	H	I	J	K	L	M	N	O	P	Q
1	?			UCP1 per mg protein - specific UCP1 content per 20 micrograms				UCP1 per mg tissue					UCP1 per depot (total protein*ucp1 per mg protein)				
2				c57	il10			c57	il10	normal			c57	il10			
3				19396	65904	969800	3295200	236536,6	983641,8	0,439589	1,828038		300974,6	563825,8	0,626369	1,173398645	
4				51531	85688	2576550	4284400	620855,4	1278925	1,153822	2,376804		445996,7	874600,1	0,92818	1,820162616	
5	20 micrograms = 0,02 mg			48684	73581	2434200	3679050	547011,2	1794659	1,016587	3,335263		510770,5	867834,1	1,062983	1,806081648	
6				63575	51089	3178750	2554450	747941,2	654987,2	1,390003	1,217253		664284,6	380708,1	1,382467	0,792305597	
7	Conteúde proteíco em um lane:							538086,1					480506,6				
8	0,02																
9																	
10																	
11			iBAT wet weight				total protein										
12			C57	IL-10	c57	Il	C57	IL-10									
13			0,082	0,067	82	67	15,51735184	8,555259									
14			0,083	0,067	83	67	8,654920804	10,2068									
15			0,089	0,041	89	41	10,49154654	11,79427									
16			0,085	0,078	85	78	10,44883431	7,45186									
17																	
18																	

Mann-Whitney test	A
	Data Set-A
	Y
1 Table Analyzed	Total UCP1 protein per BAT
2	
3 Column A	WT
4 vs.	vs.
5 Column B	IL10 KO
6	
7 Mann Whitney test	
8 P value	0.3429
9 Exact or approximate P value?	Exact
10 P value summary	ns
11 Significantly different? (P < 0.05)	No
12 One- or two-tailed P value?	Two-tailed
13 Sum of ranks in column A,B	14.00 , 22.00
14 Mann-Whitney U	4.000
15	
16 Difference between medians	
17 Median of column A	0.9956
18 Median of column B	1.490
19 Difference: Actual	-0.4942
20 Difference: Hodges-Lehmann	-0.4307

		Y
1	Table Analyzed	tissue weight
2		
3	Column A	IL10 KO
4	vs.	vs.
5	Column B	WT
6		
7	Unpaired t test	
8	P value	0.0363
9	P value summary	*
10	Significantly different? (P < 0.05)	Yes
11	One- or two-tailed P value?	Two-tailed
12	t, df	t=2.685 df=6
13		
14	How big is the difference?	
15	Mean ± SEM of column A	0.06325 ± 0.007857 N=4
16	Mean ± SEM of column B	0.08475 ± 0.001548 N=4
17	Difference between means	-0.0215 ± 0.008008
18	95% confidence interval	-0.04109 to -0.001905
19	R squared	0.5457

Mann-Whitney test	A
	Data Set-A
	Y
1 Table Analyzed	Basal Temperature
2	
3 Column A	WT
4 vs.	vs.
5 Column B	IL10 KO
6	
7 Mann Whitney test	
8 P value	0.0286
9 Exact or approximate P value?	Exact
10 P value summary	*
11 Significantly different? (P < 0.05)	Yes
12 One- or two-tailed P value?	Two-tailed
13 Sum of ranks in column A,B	26.00 , 10.00
14 Mann-Whitney U	0.0